Feedback Attenuation and Adaptive Cancellation of Blade Vortex Interaction on a Helicopter Blade Element

Kartik B. Ariyur and Miroslav Krstić

***Abstract*—Blade vortex interaction (BVI) noise has been recognized as the primary determinant of the helicopter's far field acoustic signature. Given the limitations of design in eliminating this dynamic phenomenon, there exists a need for control. We believe that this paper is the first model-based effort to attempt the same. We present herein the application, first of feedback control strategies, and then of adaptive cancellation on Leishman and Hariharan's linear aerodynamic model of a trailing edge flap. Lift fluctuations caused by vortices are taken as output disturbance. The contribution of the vortices to lift is obtained from Leishman's indicial model for gusts. The use of an active structure for actuation is assumed, and the actuator is approximated as a lag element. To design an adaptive cancellation scheme that is applicable not only to BVI but also to general problems with periodic disturbances, we start with the classical sensitivity method, and arrive at an adaptive scheme whose stability we discuss via averaging. Sacks *et al.* arrived at the same result by introducing a phase advance into a pseudogradient scheme.**

***Index Terms*—Adaptive feedforward cancellation, blade vortex interaction, feedback attenuation, indicial models, smart actuation.**

I. Introduction

HELICOPTERS radiate noise over a large frequency range, the main sources being the aerodynamic states of the main and tail rotors. Of these, the most prominent is an impulsive periodic noise that is produced under certain flight conditions, called blade slap or bang. The main cause of this noise has been identified as *blade vortex interaction* (BVI), i.e., the interaction of the blade with the vortices shed by the preceding blade(s) [5], [12], [14]. Owing to the limitations of design in prediction and control of noise, the need to meet stricter restrictions on noise in the future, and in the interest of wider applicability, the need for active control has been recognized [8]. Though there exist previous efforts in active control of BVI such as in Swaminathan *et al.* [13] we believe this is the first model-based effort.

In this paper, we use indicial response models for BVI on a helicopter blade element [4], [8]. These models assume linear aerodynamics. The aim of control is to achieve attenuation of vortex noise by control of trailing edge flaps on the blades. The idea is to alter the effective angle of attack of the flapped airfoil by altering the flap angle such that the fluctuation in lift force on the blade produced by vortex velocity is reduced. This has to be achieved without appreciably altering the thrust produced by the main rotor, the other restriction being that we have to operate within the limits of linearity of the model, i.e., small flap deflections.

In the first part of this paper, we apply *feedback* control strategies. In the second part we apply an adaptive feedforward cancellation (AFC) scheme presuming periodicity of the disturbance. To design an adaptive cancellation scheme that is applicable not only to BVI but also to general problems with periodic disturbances, we start with the sensitivity method but arrive at the same scheme derived by Sacks *et al.* [11] who introduced a phase advance into a pseudogradient scheme. We discuss stability of the scheme via averaging.

It is assumed that the control will be implemented by broad bandwidth smart actuators integrated into the rotor blades. Indeed, the motivation for this work has been the availability of such actuators in the near future. The actuator has been modeled here as a lag element. We have assumed that this lag is small (a few milliseconds).

The following section explains the indicial models used. Section III explains the control objectives and presents feedback designs, and Section III discusses simulation results with feedback control. In Section V, we detail the development of the AFC scheme, and discuss its stability for small values of the adaptation gain. In Section VI we discuss a possibility for nonconservative calculation of allowable adaptive gains and comment on the robustness of the scheme. Section VII presents simulation results with AFC.

II. Indicial Response Models

Hariharan and Leishman [4] derived the transfer functions from flap displacement (δ in Fig. 1) as the input, to lift, aerodynamic moment, and hinge moment as outputs. This model generalizes the oscillatory response of an airfoil/flap to arbitrary forcing by means of Duhamel superposition with an approximation to the indicial response function in subsonic flow. A two-term exponential approximation was arrived at by interpolating between exact values of the initial response given by piston theory and the final steady-state values given by linearized subsonic flow. The initial response to flap displacement and pitch rate were calculated through the use of aerodynamic reverse flow theorems. The model was validated by experimental data in the frequency domain.

The model gives the lift, moment, and hinge moment as the sum of circulatory and noncirculatory (inertial or apparent mass) components

$$\Delta C_L(s) = \Delta C_L^c(s) + \Delta C_L^i(s) \tag{1}$$

Manuscript received August 4, 1997; revised June 13, 1998. Recommended by Associate Editor, D. Dawson. This work was supported in part by the Army Research Office under Grant DAAH04-96-10334, the National Science Foundation under Grant ECS-9624386, and the Air Force Office of Scientific Research under Grant F496209610223.

The authors are with the Department of Applied Mechanics and Engineering Sciences, University of California at San Diego, La Jolla, CA 92093-0411 USA.

Publisher Item Identifier S 1063-6536(99)06453-2.

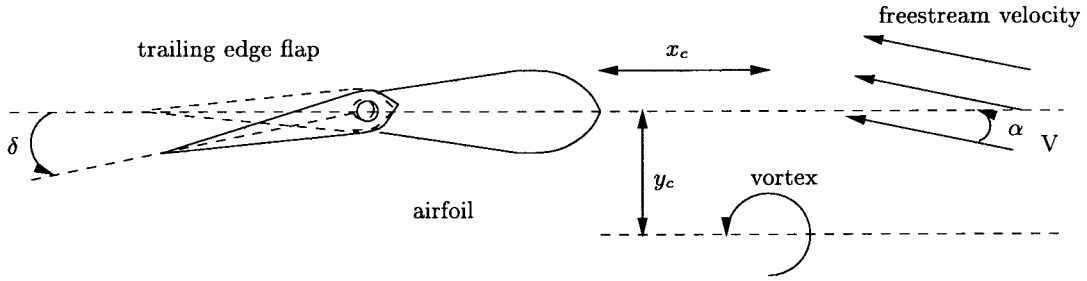

Fig. 1. Schematic of airfoil section in a BVI.

$$\Delta C_M(s) = \Delta C_M^c(s) + \Delta C_M^i(s) \quad (2)$$

$$\Delta C_H(s) = \Delta C_H^c(s) + \Delta C_H^i(s) \quad (3)$$

where the superscript c represents circulatory components and the superscript i represents noncirculatory components. The noncirculatory parts have components due to flap displacement and flap rate respectively. The signals in (1) and (2) are as follows:

$$\Delta C_L^c(s) = \left\{ k_{11} \frac{(s-z_{11})(s-z_{12})}{(s-p_{11})(s-p_{12})} \right\} \delta(s) \quad (4)$$

$$\Delta C_L^i(s) = \left\{ k_{12} \frac{s}{(s-p_{13})} + k_{13} \frac{s^2}{(s-p_{14})} \right\} \delta(s) \quad (5)$$

$$\Delta C_M^c(s) = \left\{ k_{21} \frac{(s-z_{21})}{(s-p_{21})} \right\} \delta(s) \quad (6)$$

$$\Delta C_M^i(s) = \left\{ k_{22} \frac{s}{(s-p_{22})} + k_{23} \frac{s^2}{(s-p_{23})} \right\} \delta(s) \quad (7)$$

$$\Delta C_H^c(s) = \left\{ k_{31} \frac{(s-z_{31})}{(s-p_{31})} \right\} \delta(s) \quad (8)$$

$$\Delta C_H^i(s) = \left\{ k_{32} \frac{s}{(s-p_{32})} + k_{33} \frac{s^2}{(s-p_{33})} \right\} \delta(s). \quad (9)$$

The constants $k_{11}, \cdots, k_{33}, z_{11}, \cdots, z_{31}, p_{11}, \cdots, p_{33}$ depend upon the Mach number, the freestream velocity, and the geometry of the airfoil. For further details see the Appendix.

For the modeling of the gust, we use the results derived by Leishman [8]. The transfer function from the gust velocity to the lift is of the form

$$\frac{\Delta C_{Lgust}(s)}{V_\theta^\perp(s)} = k_{gust} \frac{(s-z_{gust})}{(s-p_{g1})(s-p_{g2})} \quad (10)$$

where the constants are functions of Mach number, freestream velocity, and geometry [3], and $V_\theta^\perp$ is the component of the vortex velocity (11) perpendicular to the leading edge of the blade. The transfer function is obtained from an exponential approximation to the stationary sharp-edged gust function (indicial function). The constants were obtained by means of constrained optimization using both exact linear theory and experimental measurements [8].

For the purpose of simulation, we use Scully vortices passing the blade element at the rotor blade passage frequency, each with tangential velocity

$$V_\theta(r) = \frac{\Gamma r}{2\pi(r_c^2 + r^2)} \quad (11)$$

where Γ is the circulation, r_c is the core radius of the vortex, and $r = \sqrt{{x_c}^2 + y_c^2}$ is the radial distance from the vortex axis to the leading edge of the airfoil. (x_c, y_c) is the position of the vortex core relative to a coordinate system at the leading edge of the airfoil (see Fig. 1) where $x_c = x_0 + (V\cos\alpha)t$, $y_c = y_0 + (V\sin\alpha)t$, t is time, V is the freestream velocity, α is the angle of attack, and (x_0, y_0) is the starting point of the vortex.

III. Structure of the Noise Control System

The objective of control is to attenuate the impulsive noise of blade slap. We attempt only a reduction in the local variation in lift. On the premise that the *acoustic pressure* varies qualitatively as the *derivative of the lift*, we hope to achieve noise reduction by reducing the sharp variation in the lift due to BVI. This has to be done with minimal changes to the thrust of the helicopter. Thus, the control inputs used should be small in magnitude in comparison to the pilot pitch inputs. Also, the gust has been modeled not as input noise but as a noise addition to the output. Modeling the gust as an input noise (a disturbance in angle of attack) may be erroneous according to Leishman [8]. Thus we have a disturbance attenuation problem.

For use in the control model, we incorporate an actuator lag in series with the improper flap displacement to lift transfer function as shown in Fig. 2. The sensing of lift is assumed perfect.

The transfer function from control voltage to lift is relative degree zero, stable, and minimum phase. Thus, the use of proportional feedback, however high the gain, will not destabilize the system.

Simulation results for

1) proportional feedback;
2) linear quadratic Gaussian (LQR with a Kalman filter);
3) linear quadratic regulator (LQR) with a high gain observer

are shown and discussed in the next section.

IV. Simulation with Feedback Controllers

The results presented herein are from simulations conducted at a Mach number $M = 0.6$, a chord length $c = 1.5$ ft, a trailing edge flap width half the chord, and vortices with vorticity $\Gamma = 0.2c$ V, core radius $r_c = 0.2c$, vertical separation between vortex core and blade $y_c = 0.25c$, frequency of

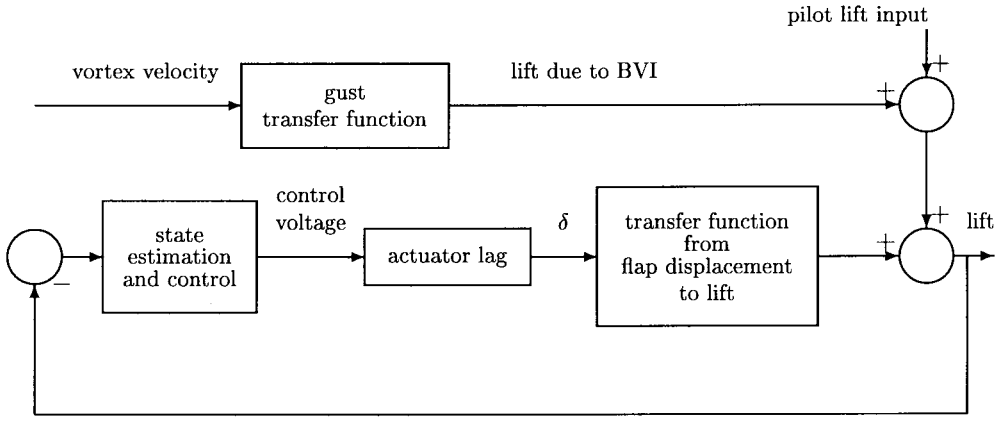

Fig. 2. Structure of the BVI control system.

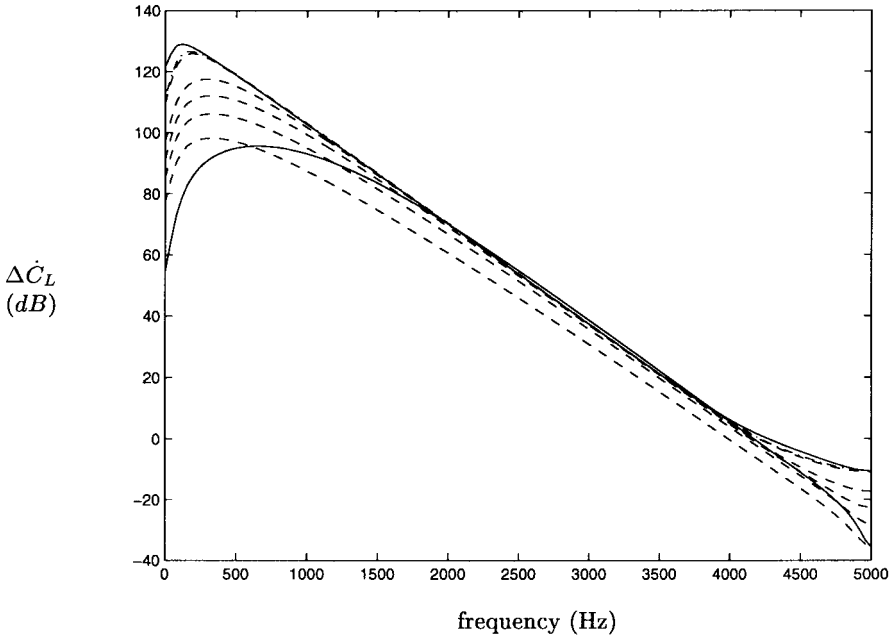

Fig. 3. Spectra of lift derivative.

BVI (equal to the blade passage frequency) $f_{bp} = 20$ Hz, and actuator bandwidth of 1800 rad/s ($\approx$286.5 Hz). A cost functional

$$J = \int_0^\infty \left[300\Delta C_L(t)^2 + u(t)^2\right] dt \tag{12}$$

where u is the control voltage applied to the actuator (see Fig. 2), was used in the linear quadratic control schemes. The rationale for the above cost functional is that we want to penalize the lift as much as possible.

Fig. 3 shows the power spectra of the lift derivative for

1) the open loop (solid line);
2) proportional feedback (dashed line—The proportional gains used were $K = 1, 5, 10, 20, 50$. The respective spectra lie one below the other);
3) LQG control (dash-dot line);
4) LQR with a high gain observer (also a solid line, the lower one)

while Fig. 4 shows the flap displacement required for

1) exact cancellation (dotted line);
2) proportional feedback (dashed line—The respective control signals (u, δ, ΔC_M, ΔC_H) for feedback gains for $K = 1, 5, 10, 20, 50$ are successively larger);
3) LQG control (dash-dot line);
4) LQR with high gain observer (solid line).

The rest of the figures use the same line types as Fig. 4.

There is a reduction of peak values of the lift and lift derivative with all the control strategies used, as is evident from Figs. 3, 5, and 6. From Figs. 3–6 it is clear that linear quadratic control with a high-gain observer outperforms low-gain proportional feedback (up to $K = 20$). LQG control performs only as well as unity feedback.

That the LQG strategy did not succeed seems to stem from a slow pole in the Kalman filter, which cannot follow the disturbance. Here, the high-gain observer, with fast poles, tracks the disturbance well and produces sufficiently large control

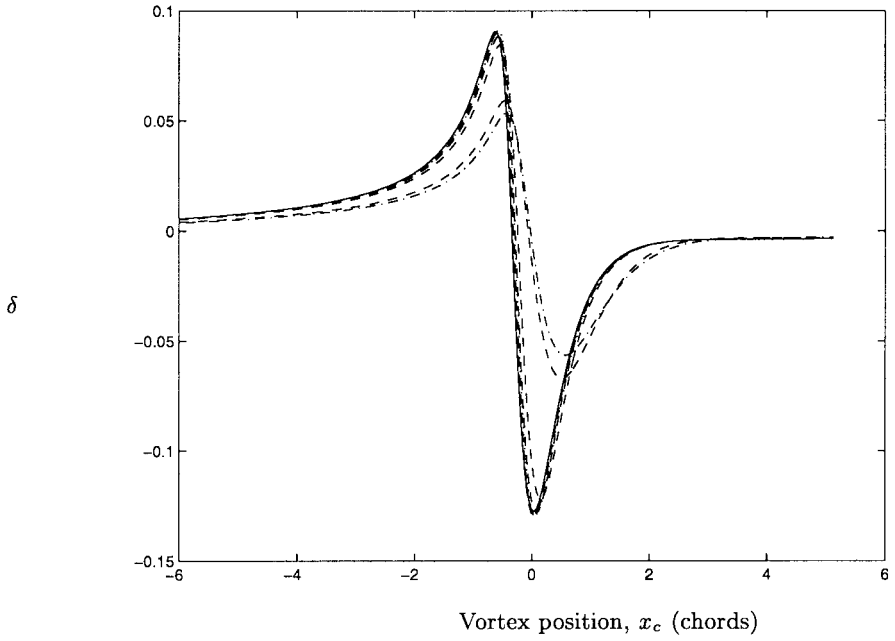

Fig. 4. Flap displacements.

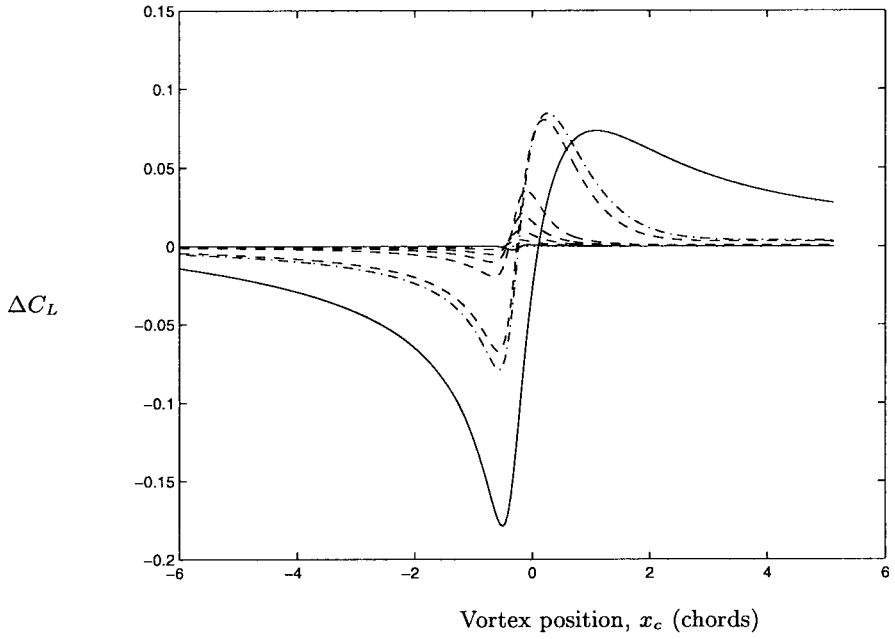

Fig. 5. Lift versus time.

inputs. Also, the feedback controls produce an improvement in performance *without exceeding the flap displacement required for disturbance cancellation* (see Fig. 4). The control strategies produce a disturbance attenuation of up to 30 dB in the frequency range of interest.

Some further underlying assumptions are that only the component of vortex velocity perpendicular to the airfoil leading edge is considered. The chordwise movement of the vortex in actual practice is not considered. Also, the reciprocal influence of the airfoil on the vortex convection velocity is neglected [8]. Thus, the BVI in which the blade cuts through the vortex is not considered. In evaluating the simulation results, it must be noted that they are only for a *blade element* and not for the entire blade.

V. Adaptive Feedforward Cancellation (AFC)

After presenting the feedback strategies, we use the periodic nature of the disturbance (the frequency of BVI being equal to the blade passage frequency) to formulate an adaptive feedforward strategy. The method in this section is applicable not only to the BVI problem but to any problem with a periodic disturbance. In the following, we consider the application of AFC in conjunction with feedback control.

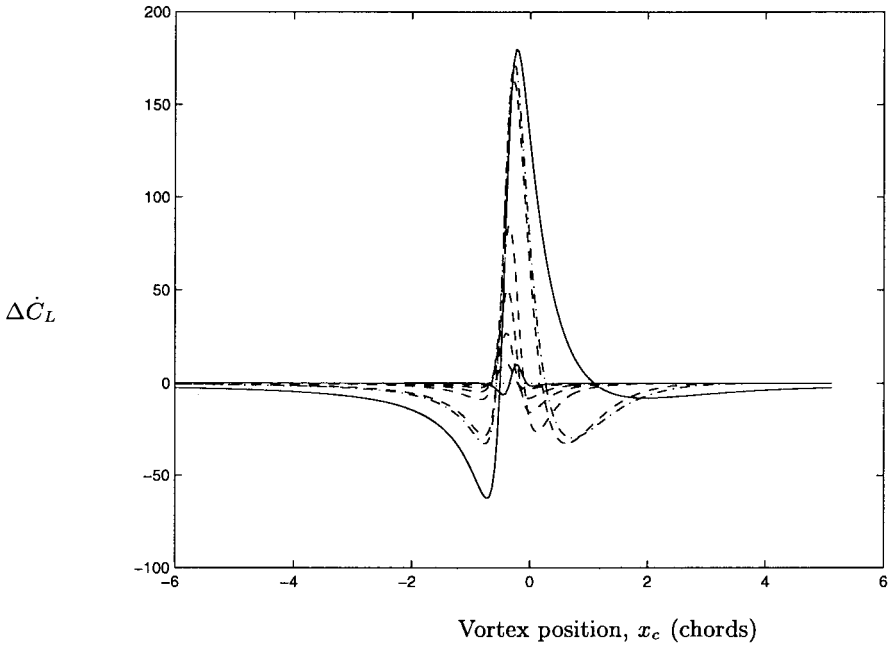

Fig. 6. Derivative of lift versus time.

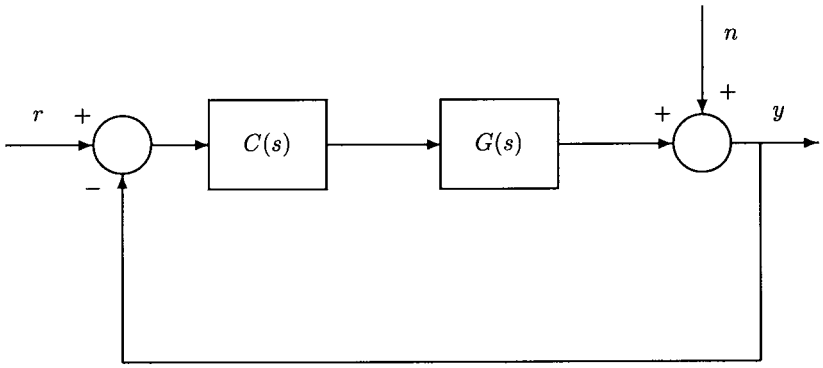

Fig. 7. A feedback attenuation scheme.

Consider the system in Fig. 7 where a feedback controller $C(s)$ has been designed for the plant $G(s)$ to achieve attenuation of the disturbance d. If we know (measure) d, the input r that we would use to cancel d is (see Fig. 8)

$$r^* = -C(s)^{-1}G(s)^{-1}d. \tag{13}$$

While it may appear that we need $C(s)$ and $G(s)$ to be minimum phase, this is not the case as we shall explain in the next section. Let us approximate r^* by the first p terms of its Fourier series

$$r^*(t) = \sum_{k=1}^{p} \{a_k^* \sin(k\omega_0 t) + b_k^* \cos(k\omega_0 t)\} = w(t)^T\theta^* \tag{14}$$

where

$$w(t)^T = (\sin(\omega_0 t) \cdots \sin(p\omega_0 t) \cos(\omega_0 t) \cdots \cos(p\omega_0 t)) \tag{15}$$

$$\theta^* = (a_1^* \quad \cdots \quad a_p^* \quad b_1^* \quad \cdots \quad b_p^*)^T. \tag{16}$$

Our task now is to find a scheme for estimating θ^* by $\theta(t)$ so that the input $r(t) = w(t)^T\theta(t)$ forces $y(t)$ to remain bounded and converge to zero. To achieve this, we employ the sensitivity method [6]. As we shall see, this approach results in the same scheme as proposed by Sacks *et al.* [11] as a phase modification of a pseudogradient scheme. The sensitivity method suggests that, in order to minimize the performance criterion $J = (1/2)y^2$, we employ the estimation of the form

$$\dot{\theta} = -\gamma\left(\frac{\partial J}{\partial \theta}\right)^T = -\gamma y\left(\frac{\partial y}{\partial \theta}\right)^T. \tag{17}$$

When y has a complicated dependence on θ, the technique in [6] would help to derive $\partial y/\partial\theta$. However, in our problem, this dependence is simple

$$y = P(s)[w^T\theta] - P(s)[r^*]. \tag{18}$$

So we obtain

$$\frac{\partial y}{\partial \theta} = P(s)[w^T] \tag{19}$$

and hence

$$\dot{\theta} = -\gamma y P(s)[w] \tag{20}$$

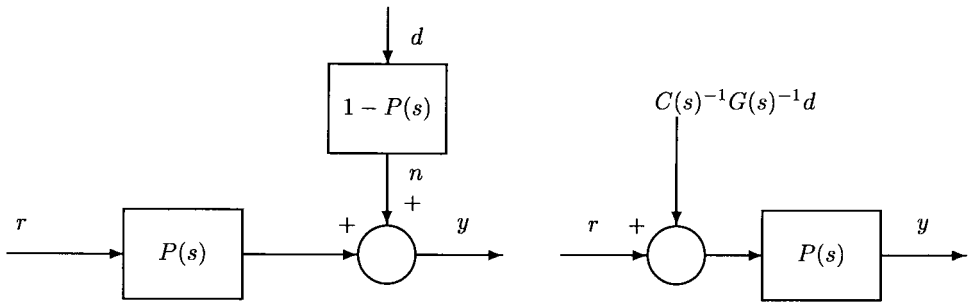

Fig. 8. Equivalent representations of the feedback attenuation where $P(s) = C(s)G(s)/1 + C(s)G(s)$.

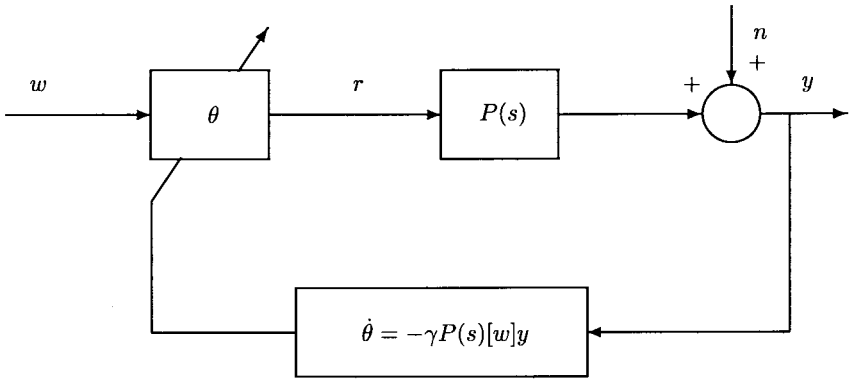

Fig. 9. AFC scheme.

where $P(s)[w] = h^T L(t) + gw(t)^T$, $L(t)$ being a matrix valued signal governed by $\dot{L} = AL + bw(t)^T$, (A, b, h^T, g) being a minimal realization of $P(s)$. The full adaptive scheme is given in Fig. 9. The implementation of the scheme is very simple because it consists of implementing $2p$ scalar equations

$$\dot{a}_k = -\gamma P(s)[\sin k\omega_0 t]y \tag{21}$$

$$\dot{b}_k = -\gamma P(s)[\cos k\omega_0 t]y \tag{22}$$

where the signals $P(s)[\sin k\omega_0 t]$ and $P(s)[\cos k\omega_0 t]$ need not be computed online.

For stability analysis, we define

$$\tilde{\theta} = \theta - \theta^* \tag{23}$$

and write (20) as

$$\dot{\tilde{\theta}} = -\gamma P(s)[w]P(s)\left[w^T\tilde{\theta}\right]. \tag{24}$$

A state-space representation of the closed-loop scheme is

$$\begin{pmatrix} \dot{x} \\ \dot{\tilde{\theta}} \end{pmatrix} = \begin{pmatrix} A & bw(t)^T \\ -\gamma P(s)[w(t)^T]h^T & -\gamma P(s)[w(t)^T]gw(t)^T \end{pmatrix} \cdot \begin{pmatrix} x \\ \tilde{\theta} \end{pmatrix} \tag{25}$$

using $y = h^T x + gw(t)^T\tilde{\theta}$. The system (25) is a linear time-varying system that is not yet in a form convenient for analysis using standard stability tools. By applying the change of variables $z = x - L\tilde{\theta}$ from Riedle and Kokotovic [10], we get

$$\dot{z} = Az + \gamma(A_1(t)z + A_2(t)\tilde{\theta}) \tag{26}$$

$$\dot{\tilde{\theta}} = \gamma(A_3(t)z + A_4(t)\tilde{\theta}) \tag{27}$$

where $A_1(t) = L(t)P(s)[w(t)]h^T$, $A_2(t) = L(t)P(s)[w(t)]P(s)[w(t)^T]$, $A_3(t) = -P(s)[w(t)^T]h^T$, and $A_4(t) = -P(s)[w(t)]P(s)[w(t)^T]$. The system (26), (27) is in a form convenient for the application of an averaging theorem from Hale [2] where $A_i(t)$ are almost periodic. We denote

$$A_4^{av} = \lim_{T\to\infty} \frac{1}{T} \int_0^T A_4(t)\,dt \tag{28}$$

and quote the averaging theorem.

Theorem 1 [2]: If A is asymptotically stable, there exists $\gamma_0 > 0$ such that $\forall\gamma \in (0, \gamma_0]$:

1) If all eigenvalues of A_4^{av} have negative real parts, then the system (26), (27) is exponentially stable.
2) If one eigenvalue of A_4^{av} has a positive real part, then the system (26), (27) is unstable.

In order to apply this theorem, it suffices to show that A_4^{av} is negative definite (note that A is asymptotically stable because $P(s)$ is stable since $C(s)$ is stabilizing for $G(s)$). The kth element of $P(s)[w]$ is $|P(jk\omega_0)|\sin(k\omega_0 t + \arg(P(jk\omega_0)))$ and its $(p+k)$th element is $|P(j(p+k)\omega_0)|\cos((p+k)\omega_0 t + \arg(P(j(p+k)\omega_0)))$. With this in mind, it is easy to see that the off-diagonal terms of $A_4(t)$ have zero average. On the other hand, the diagonal terms have the average $-(1/2)|P(jk\omega_0)|^2$, and hence

$$A_4^{av} = -\tfrac{1}{2}\,\mathrm{diag}\{|P(j\omega_0)|^2, \cdots, |P(jp\omega_0)|^2, |P(j\omega_0)|^2 \cdots, |P(jp\omega_0)|^2\}. \tag{29}$$

Since $P(s)$ is assumed to be minimum phase, it has no zeros on the imaginary axis, so $|P(jk\omega_0)|^2 > 0$ for $k = 1, \cdots, p$. Hence $A_4^{av} < 0$ and we have proved the following result.

Proposition 1: If $P(s)$ is asymptotically stable, then there exists $\gamma_0 > 0$ such that for all $\gamma \in (0, \gamma_0]$, the closed loop adaptive system in Fig. 9 is exponentially stable.

Sacks *et al.* [11] and Messner and Bodson [9] arrived at the same adaptive law. Both started from a pseudogradient update law

$$\dot{\theta} = -\gamma w(t) y = -\gamma w(t) P(s)[w(t)^T \theta] \tag{30}$$

with zero phase advance for the regressor for the purpose of cancellation of input disturbance. The stability proof for this law relies on a criterion from Riedle and Kokotovic [10], which requires that $\Re e\{P(jk\omega_0)\} > 0$. Sacks *et al.* [11] arrived at an optimal phase advance of $\arg(P(jk\omega_0))$ for the regressor from consideration of the speed of convergence of the adaptive law in an averaging analysis. Messner and Bodson [9] used a result of Bodson *et al.* [1] on the equivalence of the mapping $y \mapsto r$ to an LTI system to represent the closed loop adaptive system by a transfer function and obtained a regressor phase advance to maximize phase margin at low adaptation gain. They calculated an optimal phase advance of $\arg(P(jk\omega_0))$ by using a root-locus rule for the angle of departure of a pole from the $j\omega$-axis. The adaptive law in Sacks *et al.* [11], Messner and Bodson [9], and in our paper does not restrict the real part of the plant frequency response at the disturbance frequency to be positive.

VI. Adaptive Gains and Robustness to Higher Order Harmonics

We proceed to perform a calculation similar to that in Sacks *et al.* [11] and in Messner and Bodson [9]. We transform the equation for feedforward input

$$r(t) = \sum_{k=1}^{p} \{a_k \sin(k\omega_0 t) + b_k \cos(k\omega_0 t)\} \tag{31}$$

and the parameter update laws (21), (22) to the frequency domain using the modulation property of the Laplace transform. Substitution of the parameters in the frequency domain into the equation for $r(s)$ yields

$$r(s) = -\gamma F(s) y(s) \tag{32}$$

where

$$F(s) = \left(\sum_{k=1}^{p} \frac{\Re e\{P(jk\omega_0)\} s + \Im m\{P(jk\omega_0)\} k\omega_0}{s^2 + (k\omega_0)^2} \right).$$

From Fig. 8 we see that $y = \Pr + (1 - P)d$, which along with (32), gives

$$y = H(s) d, \tag{33}$$

where

$$H(s) = [1 + C(s)G(s)(1 + \gamma F(s))]^{-1}. \tag{34}$$

This expression allows us to draw two conclusions.

1) The order of the state-space system (26), (27) is the same as the degree of the transfer function $H(s)$. It can be shown that $H(s)$ is stable if and only if (26) and (27) are. While in Section V we proved that $y(t) \to 0$ if $d(t)$ contains exactly the harmonics we are assuming it contains, (33) and (34) allow us to conclude that $y(t)$ will be bounded for any $d(t)$—i.e., even in the presence of higher harmonics and even when the assumed frequencies are not correct (as long as γ is small). In addition, the effect of higher order harmonics on $y(t)$ would be proportional to their size. The constant of proportionality may be estimated using analysis similar to that in Kokotovic *et al.* [7].
2) One of the most interesting questions that one can pose about the results of this paper is to calculate γ_0 in Theorem 1. Estimates that would follow the analysis in [7] would be too conservative for practical use. From (34), it is obvious that a root locus calculation will enable finding permissible values for γ which are guaranteed by Proposition 1. Note, however, that for high p this calculation may become prohibitive.

VII. AFC Simulation Results

Simulation results for the AFC scheme for an adaptive gain $\gamma = 2$ and $p = 50$, with the fundamental frequency equal to a blade passage frequency of 20 Hz are shown in Fig. 10. Fig. 10 shows the spectra resulting from the application of the AFC scheme along with 1) open loop (dotted line); 2) proportional feedback (dashed lines—the line for $K = 20$ starts around 20 dB, the other gain is $K = 50$); and 3) linear quadratic control with high-gain observer (the lower solid line).

Fig. 11 shows the time history of the lift derivative when AFC is used with LQR with high-gain observer, and with proportional feedback. The slower convergence of the latter is due to the slower convergence of the adaptive parameters in θ as seen from Fig. 12. For clarity, we have shown only the coefficients $a_1, a_5, a_{10}, \cdots, a_{50}$ (bottom to top at the right end in both parts, except that the graph of a_5 in the proportional part is above that of a_{10}). Note from Fig. 10 that we do not succeed in entirely eliminating the first 50 harmonics. This is because the higher harmonics in the disturbance prevent the convergence of the adaptive parameters θ to the ideal values. That the higher harmonics modulate the adaptive parameters and produce harmonics can be seen from (21) and (22). The generation of harmonics was observed by Bodson *et al.* [1] who proposed the above explanation for it.

VIII. Conclusions and Scope for Future Work

On the basis of a linear aerodynamic model (small flap deflection) of an element of the trailing edge flap, an actuator approximated as a first-order lag, and perfect sensing of lift, we have obtained controls that produce a significant reduction in the lift fluctuations caused by blade vortex interaction. Since these sharp fluctuations are responsible for the impulsive noise, their reduction implies noise reduction. While high-gain proportional feedback performs well only with the actuator bandwidth used in the simulations, the LQR with high-gain observer almost maintains its performance with actuator bandwidth as low as 60 Hz.

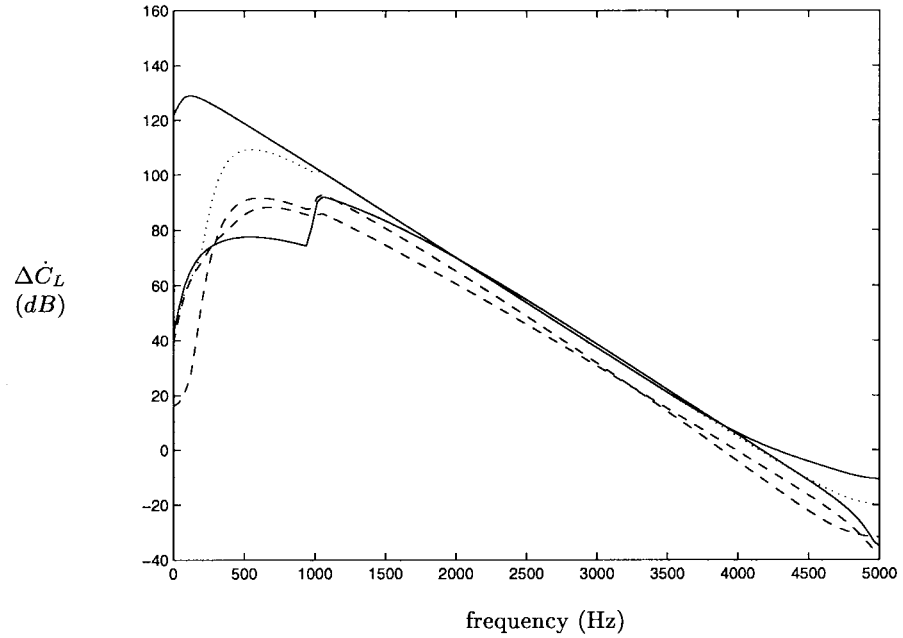

Fig. 10. AFC: Steady-state spectra.

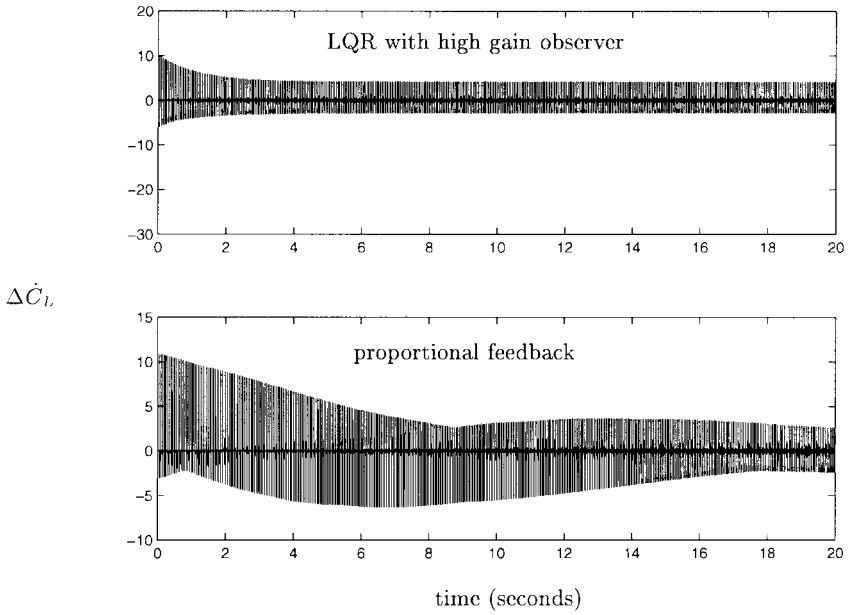

Fig. 11. AFC: Time history of lift derivative.

One advantage of the aerodynamic model used is that it is not very sensitive to changes in Mach number over its range of validity ($M \approx 0.3 \cdots 0.85$). Also, if need be, the parameters in the controller can be changed as per measurements of Mach number and freestream velocity. Also, more reliable results may be obtained if the controls are used on CFD models of the rotating main rotor.

Extensions of the above work can include incorporation of a more realistic actuator model, modeling of the sensors, the use of a model that accounts for the three-dimensional effects at the blade tip, and extension of control from the blade element to the blade. Further, the reciprocal influence between the blade and vortex (a nonlinear effect) could be considered. The rotor blade not being rigid in practice, the effects of blade flap and lead/lag motion need to be investigated, since these cause a considerable motion of the blade tip where most of the noise originates.

The most important work lies in the design of high bandwidth actuators and sensor arrays, that can withstand the rigours of the helicopter blade environment. The design requirements for the actuators can be deduced, in part from the aerodynamic and/or hinge moments they have to sustain to produce the control effort, and in part from the flap displacements desired at the frequencies under consideration.

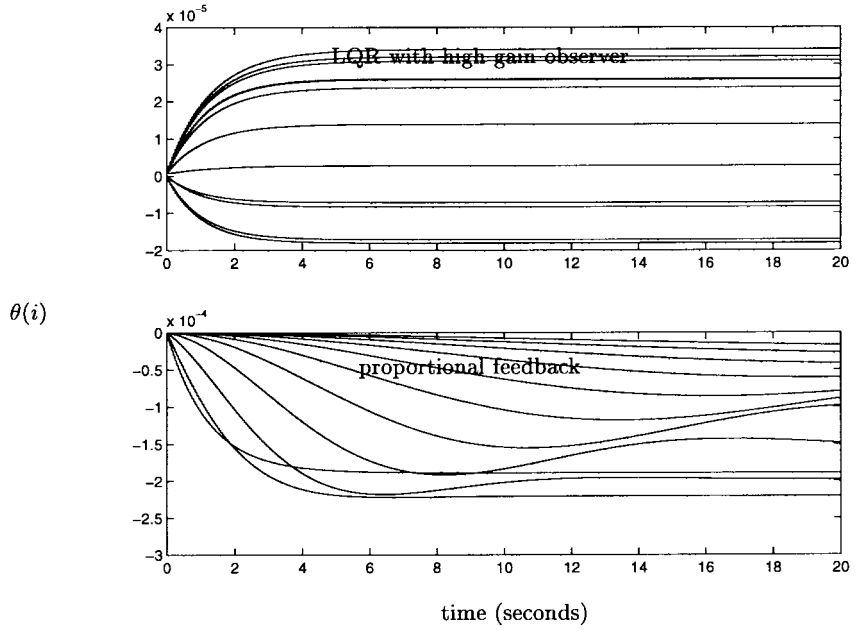

Fig. 12. AFC: Time history of parameters.

An idea that might be of use in dealing with periodic disturbances, would be to fabricate the actuator such that it has a fundamental frequency the same as the blade passage frequency.

APPENDIX
SYSTEM PARAMETERS

For completeness, we provide explicit expressions for system parameters derived in [4].

A1. Lift Transfer Function Coefficients

1) Circulatory:

$$k_{11} = \frac{f_{11}\beta}{\pi^2}(A_1 b_1 + A_2 b_2) \tag{A1}$$

$$z_{11} = \frac{b_1 b_2}{A_1 b_1 + A_2 b_2}\left(\frac{2V}{c}\beta^2\right), \quad z_{12} = \frac{2f_{10}V}{bf_{11}} \tag{A2}$$

$$p_{11} = b_1\left(\frac{2V}{c}\beta^2\right), \quad p_{12} = b_2\left(\frac{2V}{c}\beta^2\right). \tag{A3}$$

2) Noncirculatory:

$$k_{12} = \delta_1, \quad p_{13} = \frac{1}{\tau_1}, \quad k_{13} = \delta_2, \quad p_{14} = \frac{1}{\tau_2}. \tag{A4}$$

A2. Aerodynamic Moment

1) Circulatory:

$$k_{21} = \frac{-b_3}{4}(2f_1 - 2f_8 - (2e-1)f_4 + f_{11}) \tag{A5}$$

$$z_{21} = \frac{4V(f_4 + f_{10})}{c(2f_1 - 2f_8 - (2e-1)f_4 + f_{11})} \tag{A6}$$

$$p_{21} = b_3\left(\frac{2V}{c}\beta^2\right) \tag{A7}$$

2) Noncirculatory:

$$k_{22} = \delta_3, \quad p_{22} = \frac{1}{\tau_3}, \quad k_{23} = \frac{c}{V}\delta_4, \quad p_{23} = \frac{1}{\tau_4}. \tag{A8}$$

A3. Flap Hinge Moment

1) Circulatory:

$$k_{31} = \frac{b_3}{2}(f_{11}(2f_4 - f_{12})) \tag{A9}$$

$$z_{31} = \frac{2(f_5 - f_4 f_{10} + f_{12}f_{10})}{f_{11}(f_{12} - 2f_4)} \tag{A10}$$

$$p_{31} = b_3\left(\frac{2V}{c}\beta^2\right) \tag{A11}$$

2) Noncirculatory:

$$k_{32} = \delta_5, \quad p_{32} = \frac{1}{\tau_5}, \quad k_{33} = \frac{c}{V}\delta_6, \quad p_{33} = \frac{1}{\tau_6}. \tag{A12}$$

Constants $\delta_1, \cdots, \delta_6$ are the initial values of indicial response obtained from piston theory in conjunction with the reverse flow theorems. Noncirculatory time constants $\tau_1, \cdots, \tau_6$ are obtained by equating the time derivatives of the approximate solutions to the corresponding time derivatives of the exact solutions at $t = 0$ [4]. $f_1, \cdots, f_{12}$ are constants that depend on the geometry of the airfoil, and are provided by Hariharan [3]. A_1, A_2, b_1, b_2 come from the exponential approximation to the indicial lift function, $\phi_\delta^c = 1 - \sum_{i=1}^{2} A_i \exp(-b_i\beta^2 S)$, and b_3 from the approximation to indicial moment function, $\phi_{M_\delta}^c = 1 - A_3 \exp(-b_3\beta^2 S)$, where $S = 2Vt/c$ (semichords per second). c is the chord length, b is the semichord, V is the freestream velocity, M is the freestream Mach number, and $\beta = \sqrt{(1 - M^2)}$ is the Glauert factor. The coefficients A_i, b_i were obtained from experimental data in the frequency domain.

It can be noted above that the poles of the circulatory (steady-state) components of lift, aerodynamic moment, and hinge moment scale as β^2.

ACKNOWLEDGMENT

The authors wish to thank G. Leishman, J. Baeder, and I. Chopra for introducing them to the BVI problem and for fruitful discussions.

REFERENCES

[1] M. Bodson, A. Sacks, and P. Khosla, "Harmonic generation in adaptive feedforward cancellation schemes," *IEEE Trans. Automat. Contr.*, vol. 39, pp. 1939–1944, 1994.

[2] J. K. Hale, *Ordinary Differential Equations.* Malabar, FL: Krieger, 1980.

[3] N. Hariharan, "Unsteady aerodynamics of a flapped airfoil in subsonic flow using indicial concepts," Master's thesis, Univ. Maryland, College Park, 1995.

[4] N. Hariharan and J. G. Leishman, "Unsteady aerodynamics of a flapped airfoil in subsonic flow by indicial concepts," *J. Aircraft*, vol. 33, pp. 855–868, 1996.

[5] W. Johnson, *Helicopter Theory.* New York: Dover, 1994.

[6] P. V. Kokotovic, "Method of sensitivity points in the investigation and optimization of linear control systems," *Automat. Remote Contr.*, vol. 25, pp. 1670–1676, 1964.

[7] P. V. Kokotovic, B. Riedle, and L. Praly, "On a stability criterion for slow continuous adaptation," *Syst. Contr. Lett.*, vol. 6, pp. 7–14, 1985.

[8] J. G. Leishman, "Subsonic unsteady aerodynamics caused by gusts using the indicial method," *J. Aircraft*, vol. 33, pp. 869–879, 1996.

[9] W. Messner and M. Bodson, "Design of adaptive feedforward algorithms using internal model equivalence," *Int. J. Adaptive Contr. Signal Processing*, vol. 9, pp. 199–212, 1995.

[10] B. D. Riedle and P. V. Kokotovic, "A stability-instability boundary for disturbance-free slow adaptation with unmodeled dynamics," *IEEE Trans. Automat. Contr.*, vol. AC-30, pp. 102–104, 1985.

[11] A. Sacks, M. Bodson, and P. Khosla, "Experimental results of adaptive periodic disturbance cancellation in a high performance magnetic disk drive," *ASME J. Dynamic Syst., Measurement, Contr.*, vol. 118, pp. 416–424, 1996.

[12] F. H. Schmitz and Y. H. Yu, "Helicopter impulsive noise: Theoretical and experimental status," *Journal of Sound and Vibration*, vol. 109, pp. 361–422, 1986.

[13] R. Swaminathan, J. V. R. Prasad, and L. N. Sankar, "Active control of blade-vortex interactions using a neuro-fuzzy controller," in *Proc. 3rd European Conf. Smart Structures Materials*, Lyon, France, 1996, pp. 903–906.

[14] S. Widnall, "Helicopter noise due to blade vortex interaction," *J. Acoust. Soc. Amer.*, vol. 50, pp. 354–365, 1971.